Magnetic relaxation of type-II superconductors in a mixed state of entrapped and shielded flux

D. Zola,* M. Polichetti, C. Senatore, and S. Pace
SUPERMAT, INFM Regional Laboratory and Department of Physics "E. R. Caianiello," University of Salerno, via S. Allende, I-84081 Baronissi, Italy

(Received 31 July 2004; revised manuscript received 28 September 2004; published 6 December 2004)

The magnetic relaxation has been investigated in type-II superconductors when the initial magnetic state is realized with entrapped and shielded flux contemporarily. This flux state is produced by an inversion in the magnetic field ramp rate due to, for example, a magnetic field overshoot or undershoot. The investigation has been faced both numerically and by measuring the magnetic relaxation in BSCCO tapes. Numerical computations have been performed in the case of an infinite thick strip and of an infinite slab, showing a quickly relaxing magnetization in the first seconds. As verified experimentally, the effects of the overshoot (or the undershoot) cannot be neglected simply by cutting the first 10–100 s in the magnetic relaxation. On the other hand, at very long times, the magnetic states relax toward those corresponding to field profiles with only shielded flux or only entrapped flux, depending on the amplitude of the field change with respect to the full penetration field of the considered superconducting samples. In addition, we have performed numerical simulations in order to reproduce the relaxation curves measured on the BSCCO(2223) tapes; this allowed us to interpret correctly also the first seconds of the $M(t)$ curves.

DOI: 10.1103/PhysRevB.70.224504 PACS number(s): 74.25.Ha, 74.25.Qt, 74.72.−h

I. INTRODUCTION

In type-II superconductors, at temperatures $T \neq 0$, the magnetization relaxes approximately logarithmically with time (t) because of the thermally activated motion of vortices (flux creep). This behavior can be understood, at first sight, within the Anderson-Kim model[1–4] (AKM). In conventional superconductors the experimental results are well reproduced in the framework of the AKM, whereas in high-temperature superconductors (HTS's), deviations from the logarithmic decay are observed, especially in Bi-based materials.[5–8] Several models have been proposed in order to explain the nonlogarithmic relaxation.[9–13] The theory of collective creep, extensively reviewed by Blatter *et al.*,[9] predicts that the current density (J) relaxes according to the so-called "interpolation formula." As in the case of the Bean fully penetrated critical state, the magnetization can be assumed proportional to the persistent current, leading to

$$M(t,T) = \frac{M_i}{\left[1 + \frac{\mu k_B T}{U_0} \ln\left(\frac{t}{t_0}\right)\right]^{1/\mu}}, \tag{1}$$

where M_i is the initial value of the magnetization, k_B is the Boltzmann constant, and U_0 is the pinning activation energy. The exponent μ is a parameter and its value depends on the different creep regimes; t_0 is a characteristic time depending on temperature, magnetic field, sample geometry, and the fluxon attempt frequency for jumping out the pinning centers. By defining the normalized creep rate (S)

$$S = \frac{1}{M}\frac{dM}{d\ln t}, \tag{2}$$

Eq. (1) immediately leads to

$$S = \frac{-k_B T}{[U_0 + \mu k_B T \ln(t/t_0)]}. \tag{3}$$

Equation (3) is employed to evaluate experimentally the pinning activation energy and the exponent μ. For this reason, magnetic relaxation measurements are extensively used to investigate the flux creep in superconductors (for a review, see Ref. 13 and references therein).

Usually, in magnetic relaxation measurements $[M(t)]$, an external magnetic field H_a ramps up to a fixed value H_0 with finite sweep rate dH_a/dt; then, the magnetization is measured as a function of time (typically for about 10^3 s), keeping the external field at the fixed value. Ramping the external field up to H_0, which is chosen higher than the full penetration field H_p of the superconductor, screening persistent currents (clockwise with respect to the external field versus) flow everywhere in the superconductor. If the magnetic field is first increased and then slightly reduced, both clockwise and counterclockwise persistent currents flow in the sample. In this case, the measured magnetization results from a region with entrapped flux close to the surface and a region with shielded flux in the inner part of the superconductor [entrapped and shielded flux (ESF) state].

This complicated state can be easily generated when the external field ramp is stopped and a magnetic field overshoot occurs. This means that, at the nominal stop of the external field ramp, the field exceeds the target value H_0, reaching it usually after a few seconds. This overshoot can produce an entrapped flux zone close to the surface, which can appreciably affect the relaxation process. In particular, Jirsa and co-workers[14,15] showed that, for a superconducting slab of thickness 10^{-4} m in a parallel field $H_0 = 0.5$ T, an overshoot of only 1.5 mT leads to an initial magnetization M_i^{ov}, whose value is about one-third of the one computed in the absence of the overshoot. However, the depressed magnetization $M_{ov}(t)$ relaxes with time, converging to the ideal $M_{id}(t)$ curve

computed in the absence of overshoot. Therefore, the initial value of the magnetization, occurring in the absence of the overshoot, is determined approximately by extrapolating it from the long time $M(t)$ curve.

However, starting from the ESF state, the field profile evolution that leads to the joining of the two curves is still unclear. On the other hand, it is not possible to determine experimentally when the $M(t)$ curve approaches the ideal relaxation and, thus, the experimental procedure of cutting the first 10–100 s in the experimental $M(t)$ is usually adopted.

In order to justify this experimental procedure, we can consider a slab of thickness $2d$ and critical current density J_c analyzed in the framework of the Bean model. If an overshoot occurs after the application of an external field higher than the full penetration field ($H_p = J_c d$), the magnetization of the slab is[16,17]

$$M = M_{en} + M_{sh}, \tag{4}$$

$$M_{en} = (1/2)(H_{ov}^2/H_p), \tag{5}$$

$$M_{sh} = -(1/2)[(H_p^2 - H_{ov}^2)/H_p], \tag{6}$$

where M_{en} is the magnetization due to the entrapped flux, M_{sh} is the magnetization due to the shielded flux, and H_{ov} is the amplitude of the field overshoot. Equations (5) and (6) can be rewritten by introducing the magnetic reversing field H_r defined as the field amount (in absolute value), H_a has to be decreased (increased) with, for fully reversing the flux in the superconductor, if initially there was a full shielded state (entrapped state):[27]

$$M_{en} = (H_{ov}^2/H_r), \tag{7}$$

$$M_{sh} = -(1/2)\{[(H_r/2)^2 - H_{ov}^2]/H_r\}. \tag{8}$$

If $H_{ov} \ll H_p$ or equivalently $H_{ov} \ll H_r$, the magnetization due to the entrapped flux is small and thus it can be considered negligible after a long enough time. In a low T_c superconducting slab, with $d = 0.1$ mm and $J_c = 10^{10}$ A/m^2, the full penetration field is $H_p = 0.63$ T and the usual characteristic time t_0 is about 10 s. Therefore, for a few mT overshoot, it is commonly believed that the experimental $M(t)$ measured 100 s after the nominal stop of the external magnetic field resembles the relaxation from a fully shielded state (or a fully entrapped state). Nevertheless, depending on the temperature and applied magnetic field, H_p can become comparable with H_{ov}, drastically affecting also the long-time magnetic relaxation.

If we take into account the dependence of the critical current density on the magnetic field, for example, by considering the Kim dependence,

$$J_c(B) = \frac{J_{c0}}{1 + (|B|/B_k)}, \tag{9}$$

we cannot anymore write simple expressions similar to Eqs. (5) and (6).[18,19] In Eq. (9) J_{c0} and B_k are two parameters and, in particular, J_{c0} is the critical current density at zero field and B_k is the magnetic field value where J_c is half of J_{c0}. However, our discussion can be simplified if we consider that the Kim full penetration field (H_{pK}) and the Kim reversing field (H_{rK}) are given by[19]

$$\mu_0 H_{pK} = B_k(\sqrt{1+\beta} - 1), \tag{10}$$

$$\mu_0 H_{rK} = B_k(\sqrt{1+2\beta} - 1), \tag{11}$$

where

$$\beta = 2\mu_0 J_{c0} d/B_k. \tag{12}$$

In particular, if we compare H_{pK} and H_{rK} with $H_{pB} = J_{c0}d$ and $H_{rB} = 2J_{c0}d$—i.e., the Bean full penetration field and the Bean reversing field calculated for a current density field independent—we can observe that H_{pK} and H_{rK} are always lower than H_{pB} and H_{rB}. Therefore, a $J_c(B)$ leads to the overshoot (undershoot) effects on the initial magnetic state, even larger than the Bean case.

To extend the relaxation analysis to the time window affected by the overshoot, Jirsa and co-workers[14,15] have shown that it is possible to use magnetic hysteresis loop data measured at different field sweep rates. They have shown how the magnetization measured at different sweep rates can be converted into magnetic relaxation data, substantially extending the time window to the short times, typically down to 10^{-2} s.

Other complications in the analysis of relaxation measurements can also arise from the sample geometry and the anisotropic properties of the material. In fact, in HTS samples, magnetic relaxations are usually measured with the field orientation perpendicular to the largest face of the sample. In this geometry, the demagnetization effects could be neglected only for measurements performed at fields much higher than H_p. Since an overshoot changes the direction of the current and the magnetic field value on the edge of a flat superconductor, geometry effects are supposed to be significatively altered in the magnetic relaxation measurement.

In this work we have investigated the magnetic relaxation starting from a state with entrapped and shielded flux.

In the next section, we will discuss the integro-differential equation employed in the numerical computation of the $M(t)$ curves. In Sec. III, we show the numerical simulations of the magnetic relaxation and the time evolution of the field profiles for samples in the shape of the slab and thick strip.

The magnetic relaxations in BSCCO(2223) have been experimentally investigated when the effects of a magnetic field overshoot in the $M(t)$ are not negligible. Finally, in Sec. IV, the experimental measurements are analyzed and compared with the numerically computed results.

II. NUMERICAL COMPUTATIONS

In order to analyze the magnetic relaxation of a superconductor in an external magnetic field H_0, we numerically solved an integro-differential equation for the current density J in a slab in a parallel field and in a thick strip in a perpendicular field.[20] As developed by Brandt in a series of works,[20–24] in a long strip of width $2a$ (along the y axis) and thickness $2d$ (along the z axis) placed into a homogeneous

magnetic field, perpendicular to the largest face of the strip, the applied field induces surface and bulk currents. The current flows along the sample length (i.e., x axis) due to the symmetry of the strip. The induced current density $\mathbf{J}=J(y,z)\mathbf{i}$ generates a magnetic field $\mathbf{H}$ which has y and z components. In this model it is assumed that $\mathbf{B}=\mu_0\mathbf{H}$ and, thus, H_{c1} and the reversible magnetization (M_{rev}) are neglected. Since $\mathbf{B}=\nabla\times\mathbf{A}$, where $\mathbf{A}$ is the vector potential, it is possible to write for this geometry a two-dimensional (2D) Poisson equation in the Coulomb gauge:

$$\mu_0 J = -\nabla^2 A. \tag{13}$$

The current density flows only in the strip and thus the vector potential could be written as a sum of two terms $A=A_a+A_J$, where A_a is the vector potential related to the applied magnetic field ($A_a=[\mathbf{r}\times\mathbf{B}]_x=yB_a$) and A_J is related to the current induced in the strip. Since B_a is constant in the specimen, the general solution of Eq. (13) is

$$A(\mathbf{r}) = -\mu_0\int_S d^2r' Q(\mathbf{r},\mathbf{r}')J(\mathbf{r}',t) - yB_a, \tag{14}$$

where $\mathbf{r}=(x,y)$, $\mathbf{r}'=(x',y')$, and $Q(\mathbf{r},\mathbf{r}')$ is the integral kernel defined as

$$Q(\mathbf{r},\mathbf{r}') = \frac{1}{2\pi}\ln\left|\frac{\mathbf{r}-\mathbf{r}'}{r_0}\right|, \tag{15}$$

in which r_0 is an arbitrary constant length that can be chosen equal to 1. The integration is performed on the cross section of the strip S. The current density is obtained formally from[20]

$$J(\mathbf{r},t) = -\frac{1}{\mu_0}\int_{S'} d^2r' Q^{-1}(\mathbf{r},\mathbf{r}')[A(\mathbf{r}',t) + y'B_a]. \tag{16}$$

Here $Q^{-1}(\mathbf{r},\mathbf{r}')$ is the inverse kernel defined by

$$\int_S d^2r' Q^{-1}(\mathbf{r},\mathbf{r}')Q(\mathbf{r}',\mathbf{r}'') = \delta(\mathbf{r}-\mathbf{r}''). \tag{17}$$

By using the relation $\mathbf{E}=-\nabla_x\phi-\dot{\mathbf{A}}$ where ϕ is the scalar potential, we obtain

$$\dot{J}(\mathbf{r},t) = \frac{1}{\mu_0}\int_{S'} d^2r' Q^{-1}(\mathbf{r},\mathbf{r}')[E(J) - y'\dot{B}_a(t)]. \tag{18}$$

In the limit $d\gg a$ (slab geometry), the previous equation becomes a one-dimensional equation

$$\dot{J}(\mathbf{r},t) = \frac{1}{\mu_0}\int_0^a dy' Q_{slab}^{-1}(y,y')[E(J) - y'\dot{B}_a(t)]. \tag{19}$$

Taking into account the symmetry of the strip and slab geometries, the kernel in the case of the strips is given by

$$Q_{strip} = \frac{1}{4\pi}\ln\frac{(y_-^2+z_-^2)(y_-^2+z_+^2)}{(y_+^2+z_-^2)(y_+^2+z_+^2)}, \tag{20}$$

where $y_\pm=y\pm y'$ and $z_\pm=z\pm z'$. For the slab it results in

$$Q_{slab} = \frac{1}{2}(|y-y'|-|y+y'|) = -\min(y,y'). \tag{21}$$

In our simulations, we do not consider a transport current but only an external magnetic field and for this reason the term $\nabla_x\phi$ has been dropped out. To solve the integral equation for $\dot{J}$ we choose the widely used relation[25]

$$E = E_c\left(\frac{J}{J_c}\right)^n, \tag{22}$$

where J_c is the critical current density. However, the Brandt method can be used with a different E-J relationship.[20]

The current density profiles in the strip have been obtained by integrating Eq. (18), whereas for the slab Eq. (19) has been solved. For the strip, the functions J and E have been tabulated on a 2D grid with equidistant points $y_k=(k-1/2)a/N_y$ $(k=-N_y+1,\ldots,0,\ldots,N_y)$ and $z_l=(l-1/2)d/N_z$ $(l=-N_z+1,\ldots,0,\ldots,N_z)$, where $N_z=d/aN_y$ is chosen. Labeling the points (y_k,z_l) by an index i, with $i=1,2,\ldots,N$ and $N=N_yN_z$, the function $J(y,z,t)$ becomes the time-dependent vector $J_i(t)$ with N coordinates and $E(y,z,t)=E_c(J/J_c)^n$ becomes a vector with N coordinates. Moreover, the integral kernel $Q(y,z,y',z')$ becomes an $N\times N$ matrix $Q_{i,j}$.

The numerical form of Eq. (16) is

$$J_i(t+\Delta t) = J_i(t) + \frac{\Delta t}{\mu_0\Delta y\Delta z}\sum_j^N Q_{i,j}^{-1}[E_j(t) - yJ\dot{B}_a]$$

$$\text{for } i=1,\ldots,N, \tag{23}$$

where $\Delta y=a/N_y$ and $\Delta z=d/N_z$ are, respectively, the steps in the 2D grid used to tabulate the cross section of the thick strip. The numerical integration of the 1D equation for a slab follows similar rules.

The time integration of this system of nonlinear differential equations for $J_i(t)$ has to follow some prescriptions. First of all, the integration starts with the initial condition $J_i(0)=0$; in addition, the time step Δt is chosen inversely proportional to the maximum value of the resistivity $\rho_i=E_i/J_i$. Brandt[20] uses the following relation in his computations: $\Delta t=c_1/[\max(\rho_i(t))+c_2]$ with $c_1=0.3/(N_y^2 n)$, n is the exponent in the E-J law, and $c_2=0.01$. In our computations we do not use a normalized quantity and we have observed that this choice depends on the value of J_c and the time derivative of the external magnetic field. In our computations we used different values for c_1 and c_2 in order to make stable the numerical algorithm $c_1=0.003/[(N_x^2 n)\sqrt{\dot{B}_a^{\,2}}]$ where $\dot{B}_a^{\,2}$ is the temporal mean value of $\dot{B}_a$ and $c_2=1$.

Finally, $Q_{i,j}=\ln|\mathbf{r}_i-\mathbf{r}_j|$ has a logarithm divergence when $\mathbf{r}_i$ approaches $\mathbf{r}_j$. In order to avoid this singularity for $i=j$ the expression for the kernel is changed with $(1/2)\ln[(\mathbf{r}_i-\mathbf{r}_j)^2+\epsilon^2]$ where[22]

$$\epsilon^2 = \exp\left[\ln(\Delta y^2 + \Delta z^2) - \ln(4) - 3 + \frac{\Delta y}{\Delta z}\arctan\left(\frac{\Delta z}{\Delta y}\right) + \left(\frac{\Delta z}{\Delta y}\right)\arctan\left(\frac{\Delta y}{\Delta z}\right)\right].$$

In our computations, the magnetization is calculated by

$$M = 4\int_0^a dy \int_0^d dz J(y,z) y \quad \text{for a strip,} \tag{24}$$

$$M = 2\int_0^a dy J(y) y \quad \text{for a slab.} \tag{25}$$

Since the magnetic relaxation is simulated at 10^5–10^6 s, we reduce the number of computed points calculating the (t_i, M_i) data according to the relation

$$t_i = t_{i-1} + \exp[\ln(t_R)/N_R], \tag{26}$$

$$M_i = M(t_i), \tag{27}$$

where t_R is the total time of the computed relaxation and N_R is the total number of the computed data.

III. NUMERICAL RESULTS

In this section we discuss the numerical results obtained for the slab and thick strip. In our computations we have used a strip with aspect ratio (a/d) equal to 10 and $2a = 10^{-3}$ m and a slab with $2a = 10^{-4}$ m, with the critical current density (J_c) ranging from 10^6 A/m^2 to 10^9 A/m^2. The current-voltage characteristic is the usual power law given by $E = E_c(J/J_c)^n$, where $E_c = 10^{-4}$ V/m and the exponent employed, n, is chosen equal to 15 for the large creep case and $n = 105$ in the Bean limit case.

In order to study the relaxation from a ESF state, different magnetic field ramps have been taken into account. For each ramp, the external magnetic field H_a increases linearly on time, with a sweep rate $(\dot{H}_a)$ of 1 mT/s, up to a nominal fixed value H_0. The time when H_a has nominally reached H_0 is taken as time origin of the magnetic relaxation. As the external magnetic field reaches H_0, different situations are taken into account: (a) H_a is stopped immediately (ideal case), (b) H_a has a triangle overshoot (triangle overshoot), and (c) H_a has an overshoot with a smoothed field stop (exponential overshoot).

In case (b), the magnetic field increases in t_{ovm} seconds by an amplitude H_{ov}; then, it decreases by the same quantity in the subsequent t_{ov} seconds (triangle overshoot). After this, the external field is immediately stopped and the magnetic relaxation starts. In case (c), the overshoot has been simulated by means of the function $F_{ov}(t) = H_{ov}(t/t_{ovm})^c \exp[c(1 - t/t_{ovm})]$; for $t = t_{ovm}$, the overshoot reaches the maximum value. The two different functions employed to simulate an overshoot are shown in Fig. 1. For the triangular overshoot, we set $H_{ov} = 1$ mT, $t_{ovm} = 1$ s, and $t_{ov} = 5$ s. In the case of exponential overshoot, we used $H_{ov} = 1$ mT, $t_{ovm} = 1$ s, and $c = 2$. In the inset of the same figure, the time derivative of the overshoot functions are plotted, since the field ramp derivative is actually used in the integration of the diffusion equation.

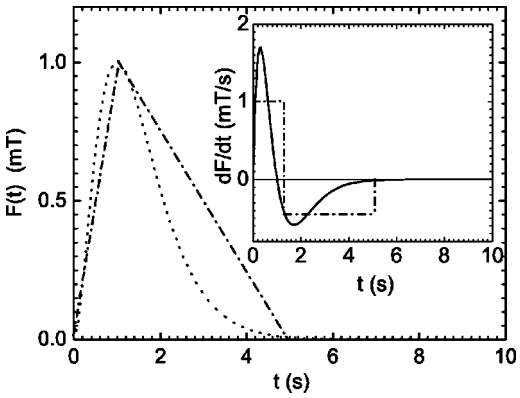

FIG. 1. Time dependence of the external magnetic field during the field overshoot. The time origin corresponds to the nominal field stop. A triangular overshoot (dash-dotted line) and an overshoot given by the function $\Delta H_{ov} = H_{ov}(t/t_{ovm})^2 \exp[2(1 - t/t_{ovm})]$ (dotted line) are shown. In the inset, the time derivatives of the two overshoot functions are shown.

We have initially computed the magnetic relaxations for a strip in a perpendicular magnetic field (perpendicular geometry) by simulating a case analogous to the one discussed in the work of Jirsa *et al.*[14] In our computation $J_c = 10^9$ A/m^2 and the critical exponent is $n = 15$. We are considering a superconductor with large critical current density but with large creep. The external field ramps with a sweep rate of 1 mT/s up to 0.2 T, which is a value well above the full penetration field of the strip. Indeed, looking at the field profile we have verified that the strip is fully penetrated for fields higher than 0.10 T. As shown in Fig. 2, also if the overshoot does not occur in the field ramp, the magnetization decays nonlogarithmically, especially at short time ($\leqslant 10$ s). This result is expected due to the power law in the *E-J* relationship which involves a logarithmic dependence of the pinning energy on the current density. In the same figure, a magnetic relaxation curve is shown as computed for a field ramp which has a triangular overshoot. In this case, the external magnetic field ramps up to 0.2 T. After this, the field overshoot occurs with an amplitude of $H_{ov} = 1$ mT. The field overshoot reaches its

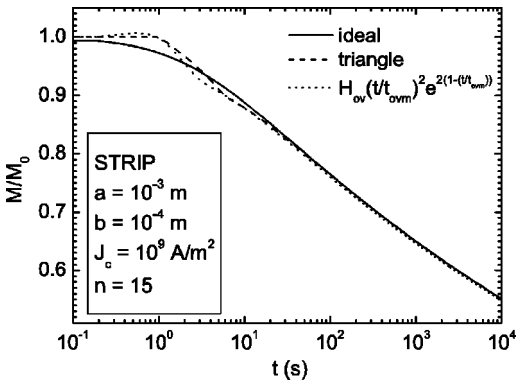

FIG. 2. Magnetic relaxation curves computed for different magnetic field ramps in a thick strip.

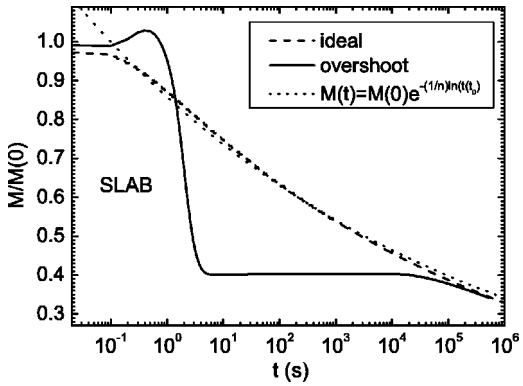

FIG. 3. Magnetic relaxation curves computed for different magnetic field ramps in a slab. The function $F_{ov}(t) = H_{ov}(t/t_{ovm})^c \exp[c(1-t/t_{ovm})]$ with $H_{ov}=1$ mT, $t_{ovm}=1$ s, and $c=2$ has been employed to simulate the field overshoot in the curve shown as the solid line. The dotted line is the relaxation given by the analytical formula reported in the text.

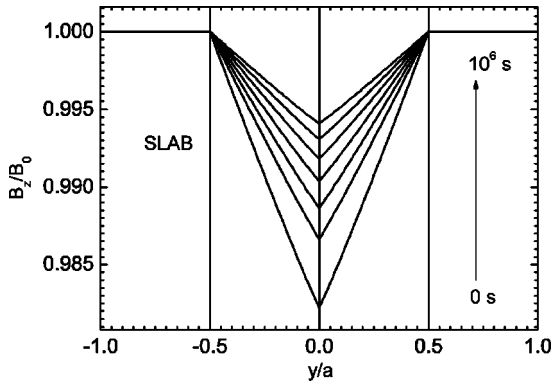

FIG. 4. Time evolution of the magnetic field profiles in a slab; the initial field profile is achieved without field overshoot.

maximum 1 s after the external field should have been stopped at the nominal target value. The external field goes down to the nominal value of 0.2 T after 5 s. Also in this case, when the magnetic field is stopped at the fixed value of 0.2 T the time derivative of H_a is instantaneously zero. A more realistic situation has been considered by computing the magnetic relaxation for case (c) where $H_{ov}=1$ mT, $t_{ovm}=1$ s, and $c=2$. Case (c) is effectively realized in experiments, where the field cannot be stopped instantaneously and the overshoot shape is rounded.

As shown in Fig. 2, the magnetization curves in cases (b) and (c) have an initial value M_i larger than in the ideal case. In fact, when the overshoot occurs, the magnetization does not relax during the first seconds, since the magnetic field continues to increase. The largest value of the initial magnetization is obtained in the case of an exponential overshoot; indeed, the electrical field induced in the superconductor in the first seconds is larger than in the other cases (see also Fig. 1). When the external magnetic field rate reverses, the magnetization quickly decreases, because of the flux coming out from the surface, and after 5 s M has lost 12% of the initial value. The decay during the first 5 s depends on the shape of the field overshoot as a function of time. In the triangular case, the magnetization curve shows a convex concavity, whereas in case (c) the curvature is concave. After 5 s, the external field is practically constant and the magnetic relaxation effectively starts; for t larger than 100 s the three curves join together. These computations confirm also in perpendicular geometry the results found for parallel geometry in Ref. 14. However, in this case the field overshoot amplitude is 1% of the full penetration field. In the next section we will consider situations where the induced ESF state strongly affects the magnetic relaxation.

A. ESF state in a slab

Here, we discuss the magnetic relaxation starting from an ESF state in the case of a slab in parallel field. In Fig. 3, two computed $M(t)$ curves are shown; the initial magnetic state is obtained by ramping the external field both in the ideal way (without overshoot) and with an overshoot of 1 mT (dashed curve). In the same figure is shown the magnetic relaxation (dotted line) for a superconducting slab, according to the relation given in Ref. 13, where it is assumed that the pinning energy depends logarithmically on the current density:

$$M(t) = M(0)\exp\left[-\frac{1}{n}\ln\left(\frac{t}{t_0}\right)\right]. \tag{28}$$

The dimension of the slab used for the computations is $2a=10^{-4}$ m, the critical current density $J_c=10^8$ A/m^2, and the exponent $n=15$. In this case the full penetration field of the slab is $H_p=6.3$ mT and thus it is of the same order of magnitude with respect to the overshoot (1 mT). As shown in Fig. 3, the computed ideal curve is approximated quite well by the analytical relation in the time range from 10 to 10^4 s, whereas it wanders off at very short and very long times. On the other hand, we observe that the overshoot has effects at a long time up to 10^5 s (dashed curve). In the first 5 s, the magnetization loses 60% of the initial value due to the inversion of the flux profile close to the slab surface. In the subsequent 10^4 s the magnetization practically does not relax, and after this time the relaxation rate increases. After 10^6 s the magnetization computed with an ideal ramp and the curve computed with a field overshoot take the same value.

At this point, it is necessary to investigate if the magnetization computed for time larger than 3.0×10^5 s in both the cases corresponds to the same magnetic state. In order to answer this question, we have computed the magnetic field profiles as a function of time. In Figs. 4 and 5, the field profiles computed for both the cases are shown. In particular, in Fig. 4, the profiles of the relaxation in a slab are shown, reproducing the usual Bean results. On the other hand, the profiles computed in the case of a relaxation from an ESF state, obtained by using the exponential overshoot change during the first 5 s (dashed line) as a consequence of the field decreasing. The evolution of the profiles during the first 5 s has some difference in comparison with the classic Bean profile, where J_c is constant and independent of the applied electrical field. In our case, while the flux is expelled on the surface, in the inner part of the slab the profile relaxes. This occurs because of the finite exponent n which leads to a large

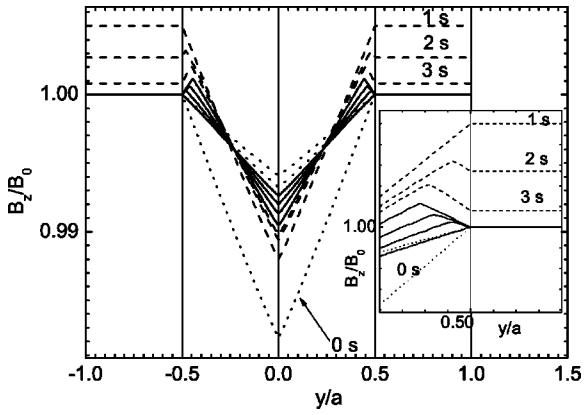

FIG. 5. Time evolution of the magnetic field profiles in a slab, when a field overshoot occurs. The dotted lines represent the flux profiles which fully resemble the ideal profiles. The dashed lines represent the profile during field ramp rate reversing. Solid lines show the field profiles in the time windows where the magnetization is nearly constant. In the inset a detail of the profile close to the slab surface is shown.

creep. On the contrary, for the Bean model, the field profile, in the inner part of the slab, remains frozen during the field decreasing.

Starting from the fifth second the field profile relaxes overall in the slab and after 10^5 s the magnetic profile becomes the ideal one. In Fig. 5 the field profiles which resemble the ideal ones are shown by dotted lines. By means of our numerical simulations we have shown that the same magnetization value found in the two $M(t)$ curves corresponds to the same magnetic state. In Fig. 5, we observe also that the maximum of the field profile, due to the field ramp rate reversing, moves towards the slab edges during the relaxation. At the same time, the entrapped magnetization is reduced down to zero. Therefore the ESF state has relaxed towards a fully shielded state.

Increasing the amplitude of the overshoot, we expect that the ideal relaxation and the relaxation from an ESF state will coincide at longer times. Nevertheless, as the region with entrapped flux prevails on the shielded region, the flux profile relaxes towards a fully entrapped state.

B. ESF state in a strip

In order to analyze the effect of the sample geometry on the relaxation, we considered the case of a strip in a perpendicular field for which the main effect of the overshoot arises on the surface, where the demagnetizing field is more intense. In Fig. 6 the magnetic field profiles for a thick strip ($2a=1$ mm, $2d=0.1$ mm) are reported; a critical current density of 10^8 A/m^2 and an E-J exponent $n=15$ are set. In the upper part of the figure we can see the field profile relaxations in the ideal case. We can observe that the demagnetizing field relaxes towards lower magnetic fields on the surface. At the same time, the field increases in the inner region and there is a boundary, known as the neutral line, where the field remains constant; it divides the region with entrapped flux from the one with shielded flux. If an overshoot of a

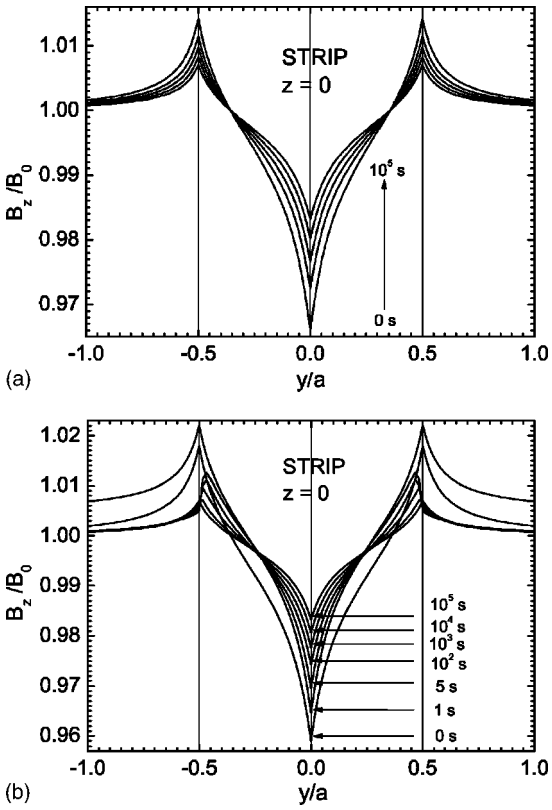

FIG. 6. Evolution field on time for a thick strip. The field profiles computed in the ideal case are shown on the upper frame. The field profiles computed when an overshoot occurs in the field ramp are shown on the lower frame.

1 mT occurs, the flux, as expected, is strongly reduced on the strip edge and the field maximum is located inside the strip. In Fig. 7 (right side), we can observe that in the next 10^6 s the maximum relaxes and moves towards the strip edge where, at the same time, the field increases. On the contrary, in the ideal case the field on the border always decreases during the relaxation as shown in the left side of Fig. 7. When the maximum reaches the edge, the field profile in the strip fully resembles the profile computed in the ideal case and the relaxation continues as in the ideal case. Also in this case, as shown in the magnetization curves in Fig. 8, the $M(t)$ with and without overshoot join together at long times. Also in the perpendicular geometry the evolution of the magnetic state is directed to rebuild a shielded state. Except for the time evolution of the magnetic field on the border of the strip, in the perpendicular geometry there are not substantial differences with respect to the parallel geometry. In fact, our computations have shown that in the perpendicular geometry, for $H_a > H_p$, the demagnetizing effects do not affect the time evolution of the magnetic relaxation.

IV. EXPERIMENTAL RESULTS AND DISCUSSION

Magnetic relaxation measurements have been performed by means of a vibrating sample magnetometer (VSM) equipped with a 16-T magnet. The external magnetic field can be ramped with a maximum sweep rate of 7 mT/s.

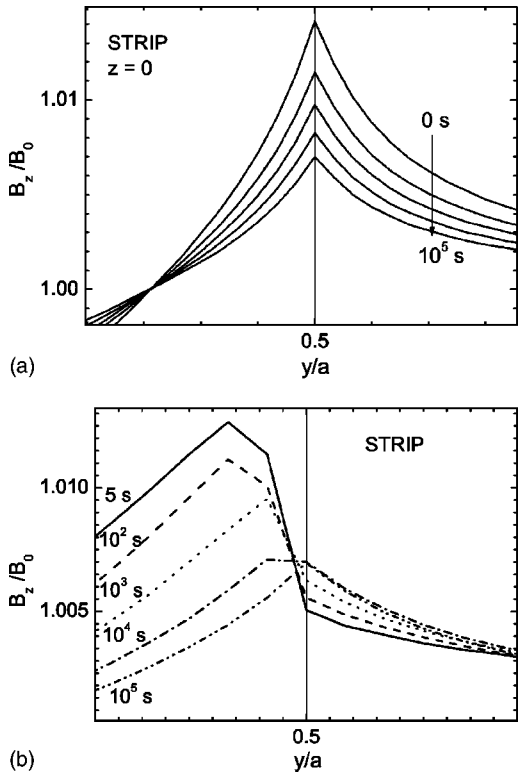

FIG. 7. Zoom-in of the previous figures, in the region close to the strip edge.

When the field is nominally stopped the magnetic field has an overshoot of around 1–5 mT depending on the sweep rate used for ramping the field and this unwanted feature has been used to induce an ESF state in our samples. We used a Hall probe to measure the time dependence of the external field and in Fig. 9 the measured undershoot for our magnet is shown when the external magnetic field ramps down to 1 T starting from 2 T with a sweep rate of 3.3 mT/s. This is the effective magnetic undershoot experienced by our samples during the experimental measurements which are discussed in the following paragraphs.

In order to check the validity of our numerical results, we have measured the magnetic relaxation on monofilamentary BSCCO(2223)/Ag tapes prepared by the standard PIT technique. We have chosen this kind of sample because they allow us to study bulk rectangular samples with full penetration fields which can be of the order of 10 mT even at the lowest temperature–i.e., 4.2 K. The dimensions of the superconducting region in the measured sample are $3.02\times0.14\times4.6$ mm^3 and the estimated critical current density ranges from 10^7 to 10^9 A/m^2, depending on the temperature. In this way we can study experimentally the overshoot effects as H_p decreases.

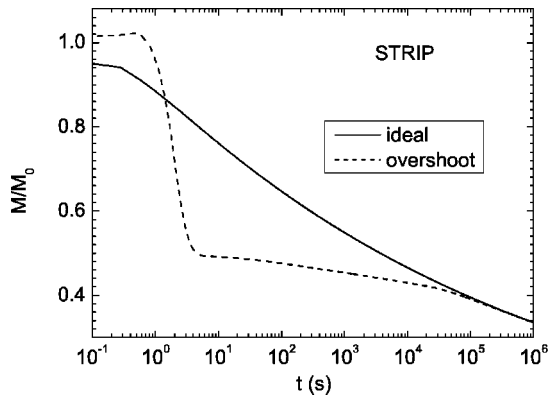

FIG. 8. Magnetic relaxation curves computed from different magnetic field ramps in a thick strip.

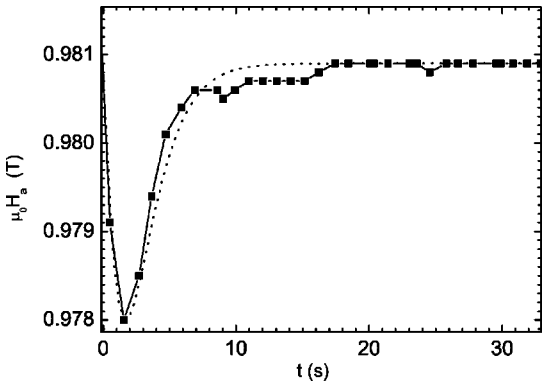

FIG. 9. Magnetic field ramp with a sweep rate of 3.3 mT/s in the time window where a field overshoot occurs, as measured by a Hall probe (squares and solid line) and $H_a(t)$ employed in our computation (dotted line).

$M(t)$ measurements have been performed with the field perpendicular to the sample surface ($H\|z$ axis) in the 4.2–45 K temperature range, cooling the sample in zero field (ZFC) for each temperature. The initial magnetic state is obtained by increasing H_a with a sweep rate of 3.3 mT/s, up to 2 T. After this, the field is decreased with the same sweep rate down to a measuring field $\mu_0 H_0 = 1$ T. The field variation of 1 T is chosen to be, for any measuring temperature, well above H_p, which is evaluated by taking the value of the field corresponding to the maximum (in absolute value) in the virgin magnetization curves at 4.2 K. In the absence of a field undershoot, a full critical state, with entrapped flux, is realized in the superconductors.[13] As the final field H_0 is nominally achieved, the $M(t)$ data are acquired each second for 5000 s.

The experimental procedure differs by the procedure employed in the numerical computations discussed in the previous sections. In the numerical simulations, we have a time saving if the initial magnetic state is achieved ramping the magnetic field from zero to H_0 because, in this way, the initial magnetic state is achieved with a lesser number of computations. On the other hand, the measured magnetization has contributions from the reversible magnetization of superconductors and also from the sample holder and, in our case, from the silver of the metallic sheet, whereas the irreversible magnetization is the only component which relaxes. Our experimental procedure enables us to measure the negative and positive branches of the magnetization curve before starting the relaxation and in this way the irreversible (M_{irr}) and reversible (M_{rev}) components of the magnetization can be evaluated[13] by using

$$M_{irr} = (M_{dw} - M_{up})/2, \tag{29}$$

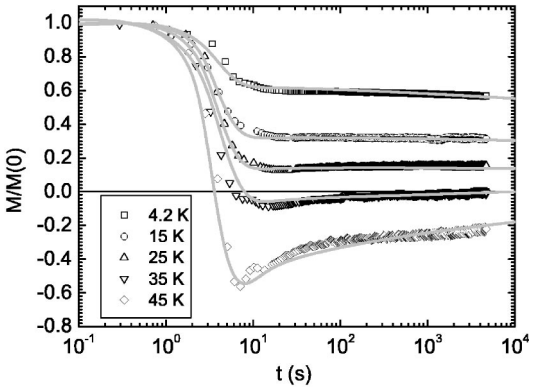

FIG. 10. Magnetic relaxations measured at different temperatures for a magnetic field $H_0=1$ T (points) and computed curves (solid lines).

$$M_{rev} = (M_{dw} + M_{up})/2, \tag{30}$$

where M_{dw} and M_{up} are the magnetization, respectively, measured in the descending and ascending branches of the hysteresis loop. In our experimental measurements we have always subtracted the measured M_{rev} and in the text we use M for the irreversible component only if not differently specified. The $M(t)$, normalized at the initial magnetization value $M(0)$, measured at different temperatures, are shown in Fig. 10. In all the curves, a large drop in the magnetization occurs during the first 11 s and this time corresponds to the time interval during which the external field has an undershoot. The behavior of the magnetization in the subsequent 5000 s depends on the value of the temperature. At 4.2 K the magnetization decreases slightly, but the relaxation after 5000 s does not exhibit the behavior expected for a fully entrapped state. At 15 K and 25 K, the magnetization remains nearly constant, whereas at 35 K and 45 K the magnetization first takes negative values and then increases in time. The effect of the undershoot increases as the full penetration field decreases with the temperature. These measurements show that the magnetic relaxation can still be affected by the field undershoot after at list 100 s. The negative values measured in the $M(t)$ at 45 K mean that the shielded flux region in the sample is larger than the entrapped one, although the initial condition was a fully entrapped state.

In order to reproduce our experimental results, we have computed the magnetic relaxation for a superconducting strip with the cross section of our sample. In the computations, the field ramp reproduces exactly the experimental field ramp, with a sweep rate of 3.3 mT/s. The undershoot has been simulated by using the exponential function discussed in Sec. III. As shown in Fig. 9, this function reproduces quite well the experimental undershoot with $H_{ov}=0.029$ mT, $t_{ovm}=1.7$ s, and $c=1.3$. In our computation we have to set both n and J_c. The exponent n has been evaluated by measuring the hysteresis loop at different sweep rates and in Fig. 11 the $M(H)$ curves measured at 4.2 K for different sweep rates are shown. Since, at first approximation, the electrical field $E \propto \mu_0 \dot{H}_a$ whereas $J \propto M_{irr}$, we can evaluate n by taking the M_{irr} values measured at 1 T for different sweep rates ($\mu_0 \dot{H}_a$)

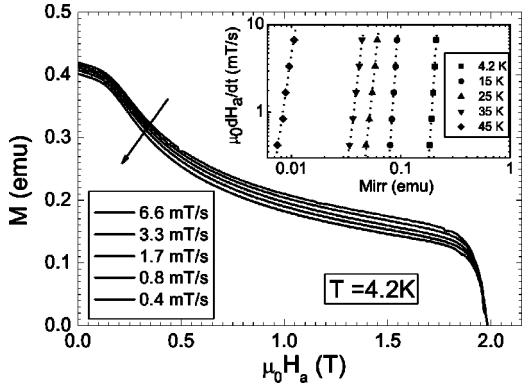

FIG. 11. Hysteresis loop measured at 4.2 K with different field sweep rate ($\mu_0 \dot{H}_a$). In the inset, the $\mu_0 \dot{H}_a$ rate versus irreversible magnetization M_{irr} is reported in a log-log scale for different temperatures as evaluated from the experimental hysteresis loop. The dotted lines are the linear fits employed to evaluate n in the *E-J* power law.

and fitting $\ln(\dot{H}_a)$ as a function of $\ln(M_{irr})$ by means of a linear fit. The experimental data and the fits for different temperatures are shown in the inset of Fig. 11. The n values reported in Table I have been rounded to the nearest integer and employed in the computations. As expected, the n values decrease for increasing temperature because n is linked to the relaxation rate[26] $S \simeq 1/(n-1)$ which increases (in the investigated temperature range) as the temperature worms up due to a larger thermally activated process.

The critical current density is a free parameter chosen in order to obtain the best fit. From our computations, it results in $J_c=2.4\times10^8$ A/m^2 at 4.2 K and 4.0×10^7 A/m^2 at 45 K. As shown in Fig. 10, the numerical computations reproduce well the experimental behavior. In Fig. 12, the profiles computed at $T=45$ K are shown. In particular, at $t=10$ s, when H_a is practically constant, it results that the magnetic state in the superconductor has both the regions with entrapped and shielded flux. In the next 5000 s, the profile relaxes toward a shielded state, which is practically fulfilled at $t=5000$ s, when the simulation is stopped.

Our work shows that the first seconds of the relaxation have to be analyzed very carefully in order to estimate correctly the creep rate and, thus, extract information about the pinning properties of the sample. In fact, our results show that it is not appropriate just to cut the first seconds of the relaxation curves and extract information from the remanent data if the presence of an overshoot in the magnet has not been previously considered.

TABLE I. Critical current densities and exponent n used for the fit of the experimental curves.

T (K)	J_c (A/m^2)	n
4.2	2.40 10^8	20
15	1.15 10^8	19
25	9.70 10^7	13
35	8.70 10^7	9
45	4.00 10^7	8

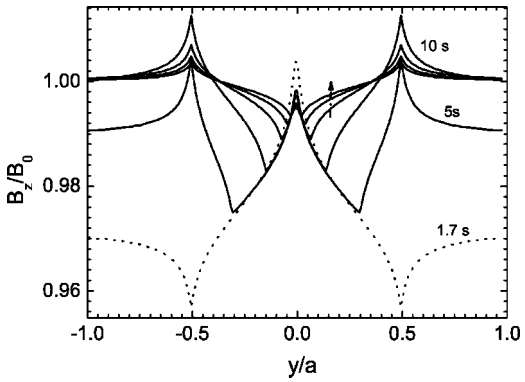

FIG. 12. Field profiles computed for the relaxation at 45 K. The profiles in the direction of the arrow are computed at $t=100, 1000$, and 5000 s.

V. CONCLUSION

In this work, we have studied the magnetic relaxation from a state with shielded and entrapped flux, generated by a field overshoot after the nominal stop of the external field. The magnetic relaxations have been computed in parallel and perpendicular geometries. The computed magnetization shows a large drop in the first seconds due to the flux expulsion from the sample boundary. After a long time, the $M(t)$ curves computed with and without field overshoot (having, thus, as initial condition an ESF and a full shielded or entrapped flux state, respectively) join together. Moreover, our simulations show that, during the relaxation, the same value of the magnetization corresponds to the same magnetic state. In addition, the experimental relaxation curves, measured on BSCCO(2223) tapes, are well reproduced by our numerical computations, allowing us to correctly analyze the $M(t)$ from the instant when the external field is nominally stopped.

ACKNOWLEDGMENTS

We thank A. Ferrentino and G. Perna for their technical support.

*Corresponding author. FAX: +3908965390. Electronic address: zoldan@sa.infn.it

[1] Y. B. Kim, C. F. Hempstead, and A. R. Strnad, Phys. Rev. **131**, 2486 (1963).
[2] P. W. Anderson, Phys. Rev. Lett. **9**, 309 (1962).
[3] P. Anderson and Y. B. Kim, Rev. Mod. Phys. **36**, 39 (1964).
[4] M. Beasley, R. Labush, and W. W. Webb, Phys. Rev. **181**, 682 (1969).
[5] H. Safar, C. Duran, J. Guinpel, L. Civale, J. Luzuriaga, E. Rodriguez, F. de la Cruz, C. Finstein, L. F. Schneemeyer, and J. Waszczak, Phys. Rev. B **40**, 7380 (1989).
[6] Y. Xu, M. Suenaga, A. R. Moodenbaugh, and D. O. Welch, Phys. Rev. B **40**, 10 882 (1989).
[7] Y. Kopelevich, S. Moehlecke, and V. V. Makarov, Physica C **249**, 144 (1995).
[8] A. A. Nugroho, I. M. Sutjahja, M. O. Tjia, A. A. Menovsky, F. R. de Boer, and J. J. M. Frause, Physica C **332**, 374 (2000).
[9] G. Blatter, M. V. Feigel'man, V. B. Geshkenbein, A. I. Larkin, and V. M. Vinokur, Rev. Mod. Phys. **66**, 1125 (1994).
[10] M. P. A. Fisher, Phys. Rev. Lett. **62**, 1415 (1989).
[11] M. V. Feiglman, V. B. Geshkenbein, A. I. Larkin, and V. M. Vinokur, Phys. Rev. Lett. **63**, 2303 (1989).
[12] R. Griessen, J. G. Lensink, T. A. M. Schröder, and B. Dam, Cryogenics **30**, 563 (1990).
[13] Y. Yeshurun, A. Malozemoff, and A. Shaulov, Rev. Mod. Phys. **68**, 911 (1996).
[14] M. Jirsa, L. Pust, H. Schnack, and R. Griessen, Physica C **207**, 85 (1993).
[15] L. Pust, J. Kadkecová, M. Jirsa, and S. Durcok, J. Low Temp. Phys. **78**, 179 (1990).
[16] C. Bean, Rev. Mod. Phys. **36**, 31 (1964).
[17] C. P. Poole, H. A. Farach, and R. J. Creswick, *Superconductivity* (Academic Press, San Diego, 1996).
[18] D.-X. Chen, A. Sanchez, J. Nogues, and J. S. Munoz, Phys. Rev. B **41**, 9510 (1990).
[19] K. Yamamoto, H. Mazaki, and H. Yasuoka, Phys. Rev. B **47**, 915 (1993).
[20] E. H. Brandt, Phys. Rev. B **54**, 4246 (1996).
[21] T. Yazawa, J. Rabbers, B. ten Haken, and H. H. ten Kate, J. Appl. Phys. **84**, 5652 (1998).
[22] E. H. Brandt, Phys. Rev. B **58**, 6506 (1998).
[23] E. H. Brandt, Phys. Rev. B **58**, 6523 (1998).
[24] Alvaro Sanchez and Carles Navau, Phys. Rev. B **64**, 214506 (2001).
[25] N. M. A. E. Zeldov, G. Koren, and A. Gupta, Appl. Phys. Lett. **56**, 1700 (1990).
[26] J. Z. Sun, C. B. Eom, B. Lairson, J. C. Bravman, and T. H. Geballe, Phys. Rev. B **43**, 3002 (1991).
[27] For a calculation of Eqs. (5)–(8) see, for example, Ref. 17, pp. 381–383, taking into account the different notations. In the formula for the flux entrapped there is correctly $1/2$ instead of $1/4$ as reported in formula (12.49) in the book.